



# Impedance analysis of $0.5\text{Ba}(\text{Zr}_{0.2}\text{Ti}_{0.8})\text{O}_3-0.5(\text{Ba}_{0.7}\text{Ca}_{0.3})\text{TiO}_3$ ceramics consolidated from micro-granules

A. Kaushal<sup>a,\*</sup>, S.M. Olhero<sup>a</sup>, Budhendra Singh<sup>b,\*\*</sup>, Duncan P. Fagg<sup>b</sup>, Igor Bdkin<sup>b</sup>, J.M.F. Ferreira<sup>a,\*</sup>

<sup>a</sup>Department of Ceramic and Glass Engineering, CICECO, University of Aveiro, 3810-193 Aveiro, Portugal

<sup>b</sup>TEMA-NRD, Mechanical Engineering Department, Aveiro Institute of Nanotechnology (AIN), University of Aveiro, 3810-193 Aveiro, Portugal

Received 17 January 2014; received in revised form 26 February 2014; accepted 8 March 2014

## Abstract

This work aims to contribute new data on the dielectric relaxation behavior of the lead-free piezoelectric  $0.5\text{Ba}(\text{Zr}_{0.2}\text{Ti}_{0.8})\text{O}_3-0.5(\text{Ba}_{0.7}\text{Ca}_{0.3})\text{TiO}_3$  (BZT–BCT) material processed in aqueous media. To obtain a BZT–BCT ceramic with high density, an aqueous suspension of BZT–BCT material was successfully transferred to spherical granules via freeze granulation, followed by sintering of a consolidated high green dens compact at 1350 °C for 4 h. The dielectric relaxation behavior in the temperature range 300–600 °C over the frequency range of 0.1 Hz–1 MHz has been carried out to display the characteristic of dielectric relaxation behavior of the BZT–BCT ceramic. Two distinct temperature dependent peaks at characteristic frequencies were observed, which shift towards the high frequency end with increasing temperature, depicting a thermally activated relaxation phenomena in the BZT–BCT ceramic. The dependences of dielectric parameters by fitting data with Cole–Cole equations (Nyquist plot) on temperature have been discussed in detail. Relaxation time was found to decrease with increasing temperature and to obey the Arrhenius relationship. The values of calculated resistances were found to be of same order for bulk ( $R_b$ ) and grain boundary ( $R_{gb}$ ) contributions, whereas capacitance values calculated for bulk ( $C_b$ ) were found to be 2 orders more than that of capacitance values calculated for grain boundaries ( $C_{gb}$ ).

© 2014 Elsevier Ltd and Techna Group S.r.l. All rights reserved.

**Keywords:** BZT–BCT ceramics; Impedance spectroscopy; AC conductivity; Electric modulus

## 1. Introduction

Recently,  $x\text{Ba}(\text{Zr}_{0.2}\text{Ti}_{0.8})\text{O}_3-(1-x)(\text{Ba}_{0.7}\text{Ca}_{0.3})\text{TiO}_3$  (BZT–BCT) with  $x=0.5$  has drawn significant attention among the various lead free piezoelectric materials due to its comparable piezoelectric coefficient to the  $\text{PbO}-\text{ZrO}_2-\text{TiO}_2$  (PZT) system with a maximum  $d_{33}$  value of 600pC/N attributed to coexisting tetragonal and rhombohedral phases near the morphotropic phase boundary (MPB) [1–8]. Lead-based ceramics are problematic due to the volatilization of PbO during sintering and due to the impact the disposal of lead-containing electronics may have on the environment. Therefore, BZT–BCT has been

regarded as a potential replacement of PZT in piezoelectric applications.

The increase in the electrical conductivity of a ferroelectric material beyond a certain temperature often restricts the utilization of several properties. The deciding factor for conductivity in the mixed B-cation perovskite system is its local defect structure that influences the short range ferroelectric ordering and acts as a variable controlling its symmetry. In addition, the electrical conduction in dielectrics is due to the ordered motion of weakly bound charge particles under the influence of an external field. Impedance spectroscopy (IS) is a non-destructive method that can correlate the structural and electrical characteristics of polycrystalline solids in a wide range of frequencies as a function of temperature [9]. It also describes the electrical processes occurring in a system by applying an a.c. signal as input perturbation, which helps to

\*Corresponding authors.

\*\*Corresponding author.

E-mail addresses: [ajay.kaushal@ua.pt](mailto:ajay.kaushal@ua.pt) (A. Kaushal), [bksingh@ua.pt](mailto:bksingh@ua.pt) (B. Singh), [jmf@ua.pt](mailto:jmf@ua.pt) (J.M.F. Ferreira).

separate the contributions of electro-active regions (such as grain boundary and bulk effects). It is particularly useful for the study of ferroelectric materials, where the ferroelectric component explains high value of the dielectric constant at the Curie temperature, by characterization of the temperature dependence variation of capacitance. Complex impedance spectroscopy consists of measuring the real and imaginary part ( $Z'$  and  $Z''$ ) of the impedance of a dielectric material at various temperatures and for different frequencies. The impedance plots of a polycrystalline sample allow the presence of grain and grain boundary properties to be resolved in the form of succession of semicircles associated with the bulk resistance ( $R_b$ ) and grain boundary resistance ( $R_{gb}$ ) of the sample, providing that their time constants differ sufficiently [10].

These properties are explained by complex parameters like complex dielectric constant ( $\epsilon^*$ ), complex impedance ( $Z^*$ ), electric modulus ( $M^*$ ), tangent loss ( $\tan \delta$ ) and conductivity ( $\sigma$ ) which are related to each as

$$Z^* = Z' - jZ'' = \frac{R}{1 + j\omega RC} \quad (1)$$

$$M^*(\omega) = M'(\omega) + jM''(\omega) = j\omega C_o Z^*(\omega) \quad (2)$$

$$\epsilon'(\omega) = \frac{Z''}{\omega C_o |Z|^2} \quad (3)$$

$$\epsilon''(\omega) = \frac{Z'}{\omega C_o |Z|^2} \quad (4)$$

$$|Z| = \sqrt{Z'^2 + Z''^2} \quad (5)$$

$$\sigma'(\omega) = \omega \epsilon_o \epsilon''(\omega) \quad (6)$$

$$\sigma''(\omega) = \omega \epsilon_o \epsilon'(\omega) \quad (7)$$

Furthermore, for all ferroelectrics, impedance spectroscopic analysis can be used to deal with several physical properties like piezoelectricity and pyroelectricity as they depend on the nature of conductivity of the material. In perovskite materials, oxygen vacancies play a predominant role in determining the electrical behavior. Thus, it would be of considerable interest to investigate the relaxation behavior of BZT–BCT to provide insights into the migration of charge defects. A better understanding of the interplay between defects and the external field can be performed to understand the role of oxygen vacancies and their contribution towards the dielectric behavior, where hopping electrons are usually inevitably involved. In our previous reports on BZT–BCT materials, we have successfully investigated the processing of electroceramic material in aqueous media [2] and the successful fabrication of BZT–BCT powder by freeze granulation. Freeze granulation has been shown to be a competitive technique for the manufacture of granules for pressing owing to its ability to preserve the particles homogeneity achieved in the suspension, thus enhancing the pressing performance [11–14]. This technology combines the advantages of colloidal suspensions, spray freezing and freeze drying that offers the possibility to produce very soft, spherical granules which show excellent flowability that allows them to be compressed into high

homogeneity compacts by dry pressing. The well controlled and self-flowing freeze granulated powders allow automated production of highly dense and defect-free green bodies by relatively quick and simple uniaxial or isostatic pressing methods. By adoption of this preparation route, several improved functional properties (structural, mechanical and electrical) of BZT–BCT ceramics on consolidation can be obtained when compared with BZT–BCT ceramics consolidated from non-freeze granulated powder [15]. In the present study, we report on the impedance analysis of BZT–BCT ceramics consolidated from freeze granulated powder. To understand the conduction mechanism in the zirconium and calcium substituted BZT–BCT composite system, the combined effect on the complex impedance and electric modulus formalisms have been reported.

## 2. Experimental details

BZT–BCT ceramic samples were prepared by using an aqueous colloidal processing route. The BZT–BCT powder was prepared by mixing appropriate molar ratios of high purity  $\text{BaCO}_3$  (Sigma-Aldrich, Steinheim, Germany),  $\text{ZrO}_2$  (Sigma-Aldrich, Steinheim, Germany) and  $\text{TiO}_2$  (Riedel-de Haen, Sielze, Germany),  $\text{CaCO}_3$  (Sigma-Aldrich, Steinheim, Germany), powders as the starting materials. The processing of BZT–BCT powder including various milling and sintering steps has been reported elsewhere [2,15,16]. A BZT–BCT aqueous suspension of 50 vol% solid loading was sprayed into liquid nitrogen ( $-196^\circ\text{C}$ ) to obtain micro-sized granules by freeze granulation (Power Pro freeze granulator LS-2, Gothenburg, Sweden). The granules were then dried at  $-49^\circ\text{C}$  under a pressure of  $1 \times 10^{-3}$  Torr in a freeze-drying system (Lab-conco, LYPH Lock 4.5, Kansas City, MO) for 72 h. The dried granules were uniaxially pressed in to disc-shaped pellets of 15 mm diameter using the isostatic pressure of 200 MPa. Finally, the sample consolidated from BZT–BCT granules was sintered at  $1350^\circ\text{C}$  for 4 h. Freeze granulation enhances the packing ability of the powder and enables achieving higher levels of green density and homogeneity in green compacts, features that improve the sintering ability and the overall properties of sintered ceramics [15,16]. Therefore, impedance data was analyzed for BZT–BCT ceramics consolidated from freeze granules. Impedance spectroscopy was performed using an Metrohm, Ecochemie-Autolab PGSTAT302N frequency response analyzer in the frequency range 1 MHz–0.01 Hz, amplitude 50 mV. For total resistance measurements, sintered BZT–BCT ceramics were painted with platinum electrodes and the measurements were carried out in an isolated chamber under in the temperature range from 600 to  $300^\circ\text{C}$  during the cooling cycle. Reliability of the results was confirmed by repeated impedance measurements at each temperature.

## 3. Results and discussion

### 3.1. Frequency and temperature dependence of $Z'$

Fig. 1a shows the variation of real part of the impedance ( $Z'$ ) with frequency at various temperatures from 300 to  $500^\circ\text{C}$

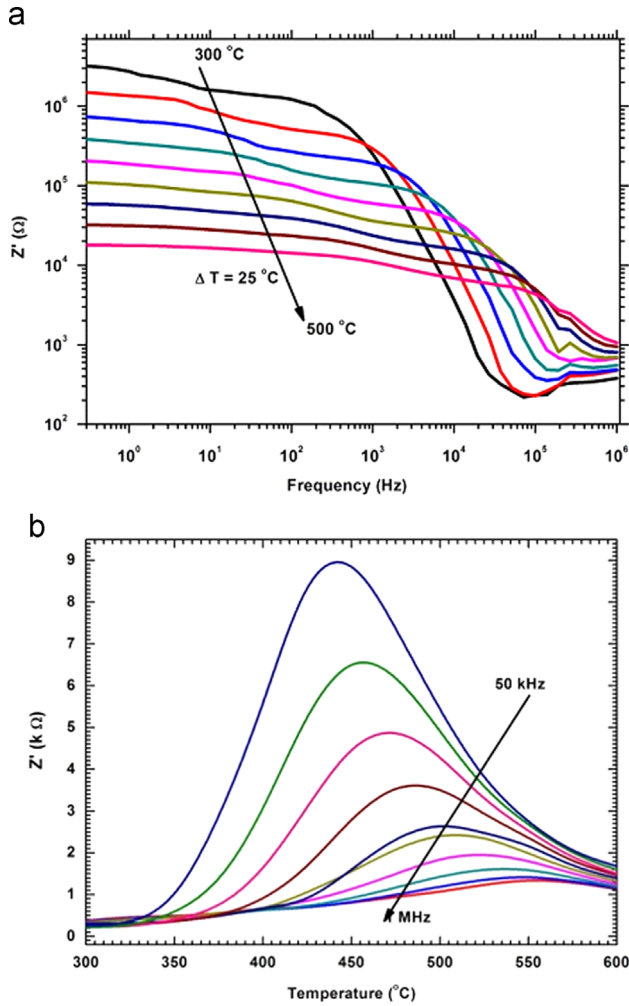


Fig. 1. Variation of real part of the impedance ( $Z'$ ) with (a) frequency and (b) temperatures in the frequency range from 50 kHz to 1 MHz and temperature range from 300 to 500  $^\circ\text{C}$ , respectively.

with temperature interval of 25  $^\circ\text{C}$ . From the plots, the values of  $Z'$  were found to decrease with increase in temperature at low frequencies suggesting a negative temperature coefficient of resistance (NTCR) [17]. In addition, the curves tend to merge together at high frequencies, leading to a temperature independent behavior at high frequencies. This may be due to the fact that the accumulated charge carriers in the vicinity of the phase boundaries have sufficient energy to pass through the barrier, leading to an enhanced conductivity with the reduction in the impedance. A decrease in the magnitude of  $Z'$  with increasing temperature also suggests an increase in the conduction process which could be due to presence of the contribution of defects associated with the ceramics. Generally,  $Z'$  is indicative of the space charge effect, which is a dominant process at low temperatures and high frequencies. On the other hand, space charge polarization is active at low frequencies and high temperatures. An increase in  $Z'$  with decreasing frequencies at around a peak temperature (as shown in Fig. 1b) can be accounted to defect concentration as well as charge accumulation at the grain boundaries. While a large decrease in real part of impedance with increasing frequency (Fig. 1a)

indicates the presence of space charge polarization [18]. The release of these space charge polarizations was observed for frequency beyond 800 kHz, where the values of  $Z'$  tend to merge together and exhibits a temperature and frequency independent behavior.

### 3.2. Frequency dependence of $Z''$

The variation of imaginary part of impedance ( $Z''$ ) with frequency at different temperatures is shown in Fig. 2a. Two distinct temperature dependent peaks at a characteristic frequency were observed for all the temperature ranges tested, which shift towards high frequency end with increasing temperature. The distinct peaks are not clearly visible for high temperatures of 425–500  $^\circ\text{C}$  due to large difference in peak intensities. Inset in Fig. 2a clearly shows two distinct peaks for high temperatures ranges from 425 to 500  $^\circ\text{C}$  which was not visible in Fig. 2a were found to shift towards high frequency. This behavior suggests a decrease in the relaxation time of the mobile charge carriers with increasing temperature and depicts a thermally activated relaxation phenomena in the BZT–BCT

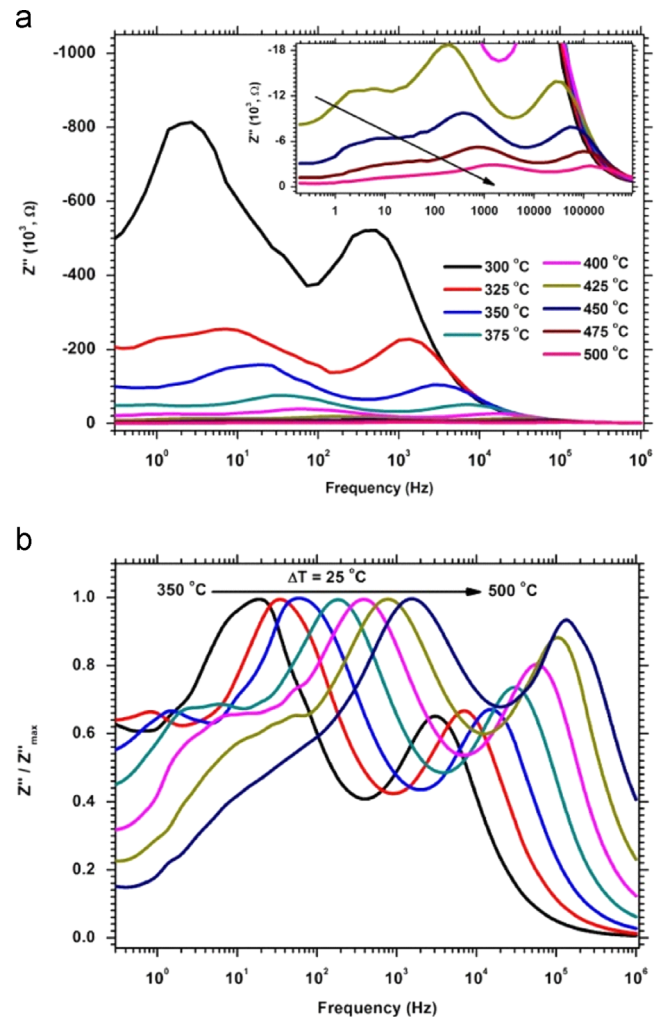


Fig. 2. Variation of (a) imaginary part of impedance ( $Z''$ ) and (b) normalized  $Z''$  with frequency at different temperatures, respectively. Inset shows two distinct peaks at high temperatures ranges from 425 to 500  $^\circ\text{C}$ .

ceramic used in the present case [19,20]. Furthermore, a sharp decrease in the  $Z''$  value with temperature illustrates a strong temperature dependence resistance of BZT–BCT ceramic. Fig. 2b shows the normalized  $Z''$  behavior with frequency. Two distinct peaks at low and high frequencies were observed. The lower frequency peak is due to the relaxation of the space charges associated with the oxygen vacancies at the grain boundary layers, whereas the higher frequency peak is attributed to oxygen vacancies relaxation inside the grains. At lower frequency, a pronounced relaxation process can be seen due to bounding of the space charges by the grain boundary. However, with increasing frequency, the space charge polarization is reduced as it becomes easier for them to relax and recombine with the vacancies in grain interiors. In addition, a broadening of the peak due to spread of relaxation times in the ceramic was also evident. These relaxation processes are due to the presence of immobile species at low temperature and associated defects (oxygen vacancies) in the ceramic at higher temperature.

In perovskite systems, the major mode of charge transport is multiple hopping processes. This hopping process normally takes place across the potential barriers set up by the lattice structure and the local environment of other atoms/ions [21].

For a thermally activated relaxation process, the relaxation time ( $\tau$ ) generally follows the Arrhenius law:

$$\tau = \tau_0 \exp \frac{E_{\text{relax}}}{k_B T}, \tag{8}$$

where  $\tau_0$  is the relaxation time at infinite temperature,  $T$  is the absolute temperature,  $E_{\text{relax}}$  is the activation energy for relaxation, and  $k_B$  is the Boltzmann constant. It is well known that at the peak position, the condition  $\omega_p \tau_p = 1$ , where  $\omega_p = 2\pi f$  is the angular frequency of measurement and the subscript  $p$  denotes values at peak position. The  $\omega_p$  values were found to increase with increasing temperature, indicating the NTCR behavior, similar to semiconductor. This semiconducting nature could be attributed to the loss of oxygen ions during high-temperature sintering process of ceramic [22].

The relaxation parameters  $E_{\text{relax}}$  and  $\tau_0$  were determined by plotting  $\ln(\omega_p)$  as a function of the inverse of temperature and fitting using Eq. (8) (Fig. 3). The values of activation energy for relaxation for bulk and grain boundary were found to be 1.118 and 1.226 eV, respectively. This strongly suggests that the electrical behavior in the present case is influenced by the polarization phenomenon and that the conduction mechanism is of the hopping type [23,24].

Fig. 4 shows the complex impedance plots of  $Z'$  versus  $Z''$  (Nyquist plot) at different temperatures. The complex impedance plots are characterized by successive semi-circular arcs of grain, grain boundary and electrode contributions, and each arc is represented by a parallel combination of two  $RQ$  elements, where  $R$  and  $Q$  are the resistance and the constant phase element of the circuit. The shape and the width of the arc indicate the type of relaxation mechanism for the system. In the present case depressed semicircles were observed indicating a distribution of the relaxation time. This suggest that the arc cannot be fit using an ideal capacitor  $C$ , and should be replaced by a constant phase element (CPE)  $Q$  defined as [25]

$$Z_Q^* = \frac{1}{(i\omega)^n C} \tag{9}$$

where,  $n$  is the empirical exponent and its value varies from 0 to 1; for an ideal capacitor  $n=1$  and for an ideal resistor it is 0. The Nyquist plot for BZT–BCT ceramic obtained at different

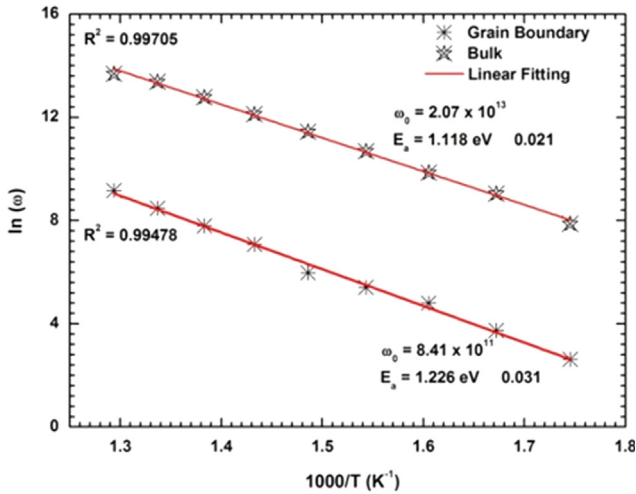


Fig. 3.  $\ln(\omega_p)$  variation as a function of the inverse of temperature.

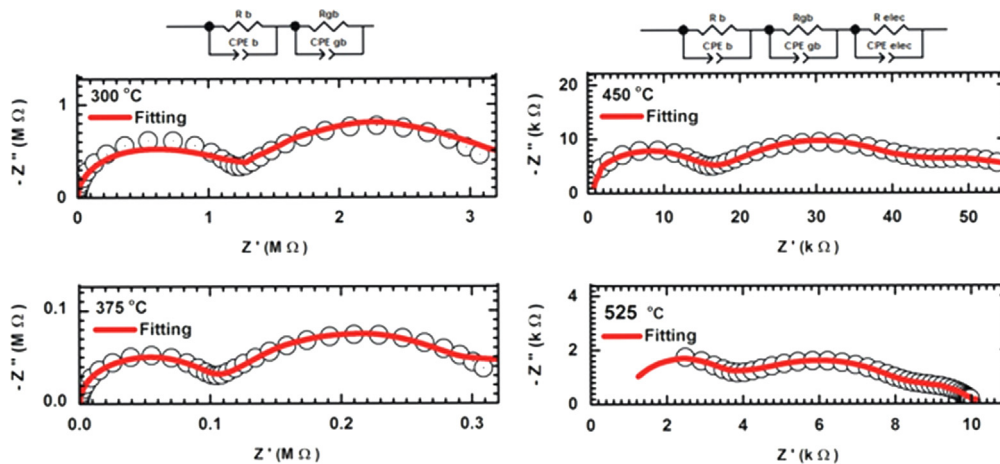


Fig. 4. Complex impedance plots of  $Z'$  versus  $Z''$  (Nyquist plot) at different temperatures of 300, 375, 450 and 525 °C.

temperatures in the frequency range 0.1 Hz–1 MHz were found to exhibit two semi-circular arcs till 375 °C due to bulk (grains) and grain boundary contributions in sequence. However, at higher temperature (at  $\geq 400$  °C) and at very low frequency, the observed behavior is due to the electrode contribution. The complex impedance data have been analyzed for two temperatures below 400 °C (i.e. 300 °C and 375 °C) and two temperatures above 400 °C (i.e. 450 °C and 525 °C) by considering the equivalent electrical circuit of  $RQ$  elements connected in series, as shown in Fig. 4. The equivalent circuit best fitted to experimental data consists of two  $RQ$  elements for temperatures below 400 °C and three  $RQ$  elements for temperatures above 400 °C. The solid lines shown in Fig. 4 indicate the best fit with the experimental data points. The obtained fitting parameters are shown in Table 1. The true values of capacitance for bulk and the grain boundary were calculated using the relation as [26,27]

$$C = (R^{1-n} Q)^{\frac{1}{n}} \quad (10)$$

The sample resistance was found to decrease with rise in temperature which suggests a negative temperature coefficient of resistance (NTCR) and indicating a typical semiconducting behavior of BZT–BCT ceramic. Furthermore, the fitting results showed a higher value of  $R_{gb}$  (grain boundary resistance) as compared to  $R_g$  (grain resistance) due to a lower concentration of oxygen vacancies and trapped electrons in grain boundaries. This can be explained as; the creation of oxygen vacancies and other charge carriers (e.g., electrons and holes) are related to process parameters at various stages like calcination and sintering during the synthesis of the material at high temperatures. These defects greatly influence the conduction and dielectric relaxation behavior. During sintering at high temperature, oxygen loss increases leading to the formation of oxygen vacancies as  $2O_O^x \rightarrow O_2(g) + 2V_O + 4e^-$ . However, when temperature is slowly cooled to room temperature in air, a re-oxidation process occurs as  $2V_O + O_O^x + 4e^- \rightarrow O_2(g)$ . The occurrence of this re-oxidation process at the grain boundaries leads to the formation of an insulating grain boundary and highly conductive oxygen deficient grains [28]. The relaxation time ( $\tau$ )

associated with bulk and grain boundary were calculated using relation,  $\tau = RC$ . The relaxation time was found to decrease with increasing temperature suggesting a temperature dependent relaxation process in the BZT–BCT ceramic and is related with Eq. (8).

Fig. 5a shows the variation of relaxation time ( $\tau$ ) for bulk and the grain boundary with inverse of temperature. The activation energy for relaxation associated with the bulk and grain boundary were calculated from linear fitting as shown in Fig. 5a and found to be 1.121 and 1.301 eV for bulk and grain boundary, respectively. From the fitted values as obtained from Nyquist plot, the dc conductivity ( $\sigma_{dc}$ ) due to bulk and grain boundary at different temperatures were calculated using the relation

$$\sigma_{dc} = \frac{d}{RA} \quad (11)$$

where,  $d$  and  $A$  are the thickness and surface area of the electrode and  $R$  is the resistance. Fig. 5b shows the variation of  $\sigma_{dc}$  for bulk and grain boundary as a function of inverse of temperature. The  $\sigma_{dc}$  in both cases was found to increase with temperature. The curve was fitted with Arrhenius equation for conduction given by

$$\sigma = \sigma_o \exp\left(\frac{E_a}{k_B T}\right), \quad (12)$$

where,  $E_a$  is the activation energy,  $k_B$  is the Boltzmann's constant and  $\sigma_o$  is pre-exponent factor. The activation energy for conduction for bulk and grain boundary was found to be 0.994 and 1.106 eV, respectively. These calculated values of activation energies are very close to that for oxygen vacancy conduction in perovskite system ( $\sim 1$  eV) which suggests that the conductivity in the present case is governed by the oxygen vacancies in the BZT–BCT ceramic. Further, a very low difference between these activation energies (0.112 eV) suggests a small potential barrier between the grain and grain boundary. A significant low value of barrier height suggests a relatively high density of BZT–BCT ceramic as obtained due to a finely processed freeze granulation process with a very low order of grain coarsening [29,30,16].

Table 1

Calculated values of capacitance, resistance and relaxation time for bulk and the grain boundaries of BZT–BCT ceramic sintered at 1350 °C for 4 h.

Temp (°C)	Bulk				Grain boundary				Relaxation time	
	$R_{bulk}$ (k $\Omega$ )	$Q_{bulk}$ (pF)	$n$	$C_{bulk}$ (pF)	$R_{gb}$ (k $\Omega$ )	$Q_{gb}$ (nF)	$n$	$C_{gb}$ (nF)	$\tau_{bulk}$ ( $\mu$ s)	$\tau_{gb}$ ( $\mu$ s)
300	1160	302	1.00	291	2230	50.6	0.77	25.90	337.00	57600
325	445	252	1.00	252	978.56	45.3	0.78	18.90	112.00	18500
350	197	227	1.00	227	506.27	77.1	0.72	21.62	44.80	10900
375	94.48	210	1.00	210	243.26	100	0.69	19.52	19.80	4750
400	48.29	194	1.00	194	116.17	118	0.69	17.30	9.38	2010
425	25.47	182	1.00	182	60.85	139	0.68	14.43	4.63	878
450	14.07	176	1.00	176	31.49	183	0.66	12.65	2.48	398
475	8.15	172	1.00	172	17.37	230	0.64	10.97	1.40	191
500	5.63	574	0.91	159	8.29	166	0.71	11.24	0.89	93
525	3.43	309	0.95	158	4.99	213	0.69	9.52	0.54	48
550	2.34	284	0.94	115	2.86	165	0.70	6.43	0.27	18
575	1.76	783	0.87	112	1.55	131	0.75	7.40	0.20	11.4

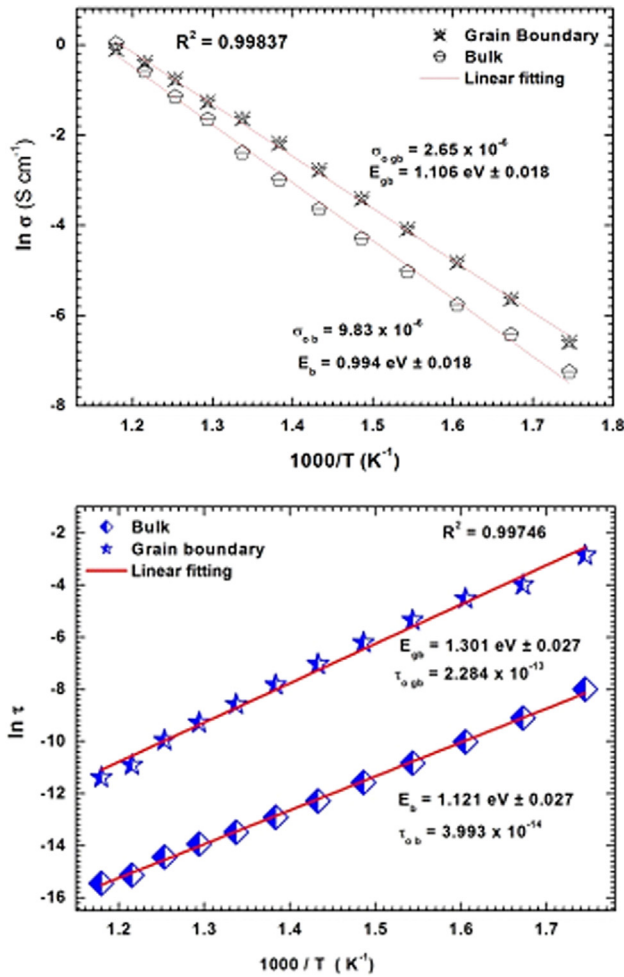


Fig. 5. Variation of (a) relaxation time ( $\tau$ ) and (b) dc conductivity ( $\sigma_{dc}$ ) for bulk and the grain boundary with inverse of temperature.

### 3.3. AC conductivity analysis

Fig. 6 shows the variation of ac conductivity ( $\sigma_{ac}$ ) with inverse of temperature at different frequencies. A sharp increase in the ac conductivity was observed for the sample suggesting strong temperature dependence of ac conductivity of BZT–BCT ceramic. Further, at low temperature a larger difference in the ac conductivity with increasing frequency (higher at higher frequency) was observed which converges at high temperature (Fig. 6). The convergence of ac conductivity with a very small difference in conductivity values at relatively higher temperature suggests a frequency independent behavior of BZT–BCT ceramic at high temperatures. The curve was fitted with Arrhenius equation for conduction using Eq. (12) and the values of activation energy for ac conduction at different frequencies were calculated from the slope of the curve. The inset in Fig. 6 shows the variation of the activation energy as a function of frequency. A gradual decrease in the ac conductivity from 1.03 to 0.84 eV was observed with increase in frequency from 10 Hz to 10 kHz, respectively. A similar kind of behavior has also been reported for lead based perovskite [21].

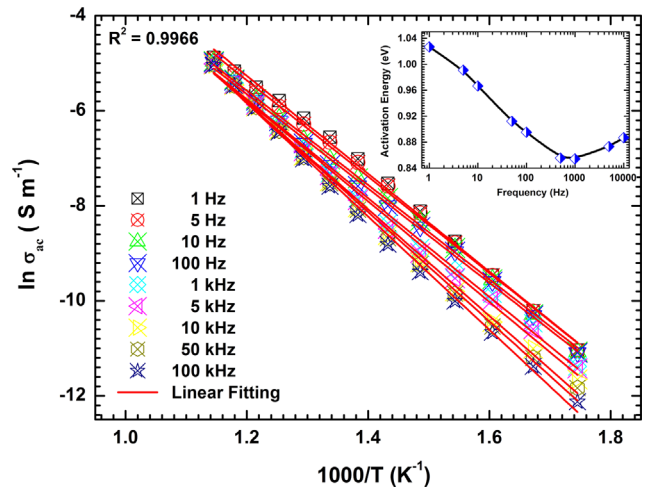


Fig. 6. Variation of ac conductivity ( $\sigma_{ac}$ ) with inverse of temperature at various frequencies. The inset shows the variation of the activation energy as a function of frequency.

### 3.4. Electric modulus

The character of the high frequency, bulk response was studied in more detail using plots of real part of electric modulus ( $M'$ ) and imaginary part of electrical modulus ( $M''$ ) versus  $\log(f)$  at different measuring temperatures range from  $300^\circ\text{C}$  to  $600^\circ\text{C}$ , as shown in Fig. 7a and b. Using the impedance and electric modulus formalism, one can understand the complete nature of the bulk ceramic [31]. An increase in the peak height of  $M''$  was observed with increasing temperature which is due to decrease in the capacitance with increasing temperature and is a characteristic feature of a ferroelectric material in the paraelectric region above  $T_c$ . The peaks were also found to shift systematically towards higher frequency with increase in temperature as shown in Fig. 7. The frequency range below the peak frequency determines the frequency range in which charge carriers are mobile over a long distance whereas frequency range above the peak frequency, the charge carriers are confined to a potential well and are mobile over short distances [32]. The relaxation time ( $\tau$ ) for BZT–BCT ceramic was estimated from the peak frequency as  $\tau = 1/\omega = 1/2\pi f_r$ , where  $f_r$  is value of frequency at peak position observed in Fig. 7b. The magnitude of  $\tau$  values was found to be of the order of  $10^{-14}$  s, which suggests a hopping conduction mechanism in the investigated BZT–BCT ceramic. The activation energy was calculated from the slope of  $\log(\tau)$  versus inverse of temperature using the Arrhenius Eq. (8) and is shown in inset of Fig. 7b. The value of activation energy was calculated to be 1.221 eV. A small variation in frequency values of peak position has been observed when compared to peak positions observed at various measured temperatures range for normalized impedance behavior with frequency (Fig. 2b). This deviation in frequency values at peak position for normalized impedance and electric modulus at different temperatures indicates a short range conductivity process in the system

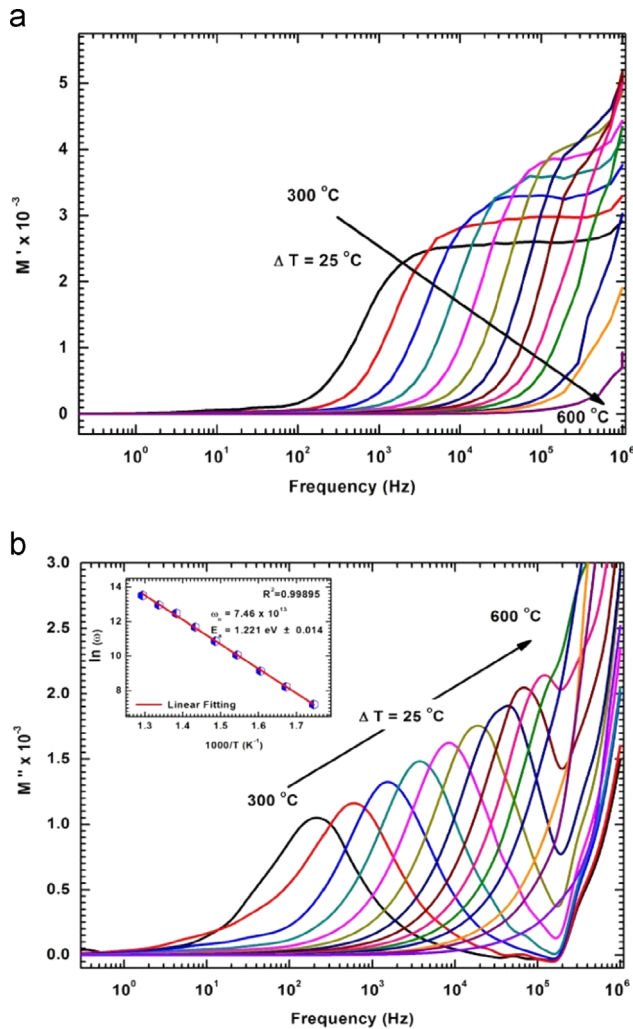


Fig. 7. Plots of (a) real part of electrical modulus ( $M'$ ) and (b) imaginary part of electrical modulus ( $M''$ ) versus  $\log(f)$  at different measuring temperatures range from 300 °C to 600 °C.

whereas in general, for non-localized (long range) conduction process these peaks must overlap with matching in frequency values at peak positions. In addition, this mismatch of two distinct curves also suggests the polarization process due to localized conduction of multiple carriers and confirms the presence of multiple relaxation process in BZT–BCT ceramic. Furthermore, a contribution of lattice defect and/or structural aspects in the conduction mechanism was evident from an asymmetry in the curve found above the frequency of maxima (Fig. 7).

Fig. 8 shows the complex electric modulus plots of  $M'$  versus  $M''$  at different temperatures which shows only one semicircular arc type behavior compared to two successive semicircular arcs observed in case of impedance formulation (Fig. 4). This could be due to a significantly large difference in the  $\tau$  values calculated at different temperatures for bulk and the grain boundary as the  $\tau$  values for the grain boundary is approximately 100 times more than that of  $\tau$  values for bulk (Table 1). The values of resistances calculated were found to be of same order for bulk ( $R_b$ ) and grain boundary ( $R_{gb}$ )

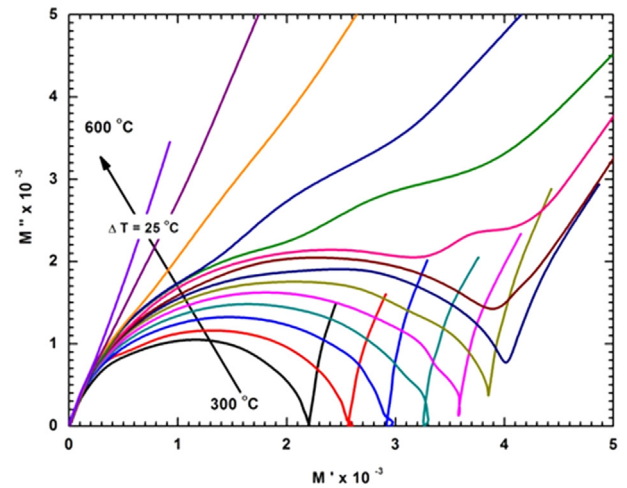


Fig. 8. Complex electric modulus plots of  $M'$  versus  $M''$  at different measured temperatures in the range from 300 to 600 °C.

contributions, whereas capacitance values calculated for bulk ( $C_b$ ) were found to be 2 orders more than that of capacitance values calculated for grain boundaries ( $C_{gb}$ ). This big difference in calculated  $C_b$  and  $C_{gb}$  values of BZT–BCT ceramic reveal that, at high temperature the electric behavior of BZT–BCT ceramic is purely dominated by the capacitance effect. Due to this, in the present case it is expected that both the RC elements response (viz due to grain and grain boundary) would not appear in the electric modulus plot. When the behavior is dominated by resistance, the electric modulus shows both RC elements, whereas the impedance plots reveal only one [33]. On contrary to this, if the behavior is dominated by capacitance, the contribution from both the RC elements could be observed in impedance plot whereas it would be absent in electric modulus plot. This is due to the fact that the magnitude of the  $Z''$  is proportional to the magnitude of Resistance ( $R$ ), while the  $M'$  is proportional to the inverse of capacitance ( $1/C$ ). The modulus plots highlight the smallest RC element and the impedance plots are dominated by RC element with maximum resistance. Hence, in the electric modulus plot (Fig. 8) we found only the contribution due to bulk rather than both bulk as well as grain boundary contributions as observed in impedance plot (Fig. 4). This suggests that the occurrence of the peak in the electric modulus plot is dominated by the bulk contribution. A small difference in the activation energy for relaxation from electric modulus and impedance modulus plots is, therefore, possibly due to the aforementioned difficulty of resolution between bulk and grain boundary responses using this formulism.

#### 4. Conclusions

Stable aqueous suspension of lead free piezoelectric material of composition  $0.5\text{Ba}(\text{Zr}_{0.2}\text{Ti}_{0.8})\text{O}_3-0.5(\text{Ba}_{0.7}\text{Ca}_{0.3})\text{TiO}_3$  (BZT–BCT) were successfully transformed to micro granules via spraying a stable aqueous suspension into liquid nitrogen (freeze granulation), followed by freeze drying. The complete impedance spectroscopy of sintered BZT–BCT ceramic consolidated from granulated

powder is analyzed. Nyquist plots show both grain and grain boundary contributions to impedance. It also shows that bulk resistance ( $R_b$ ) decreases with increase in temperature, manifesting the NTCR behavior of the compound. Relaxation time was found to decrease with increasing temperature which follows the Arrhenius relationship. The electrical relaxation process occurring in the material has been found to be temperature dependent.

## Acknowledgments

Authors, A. Kaushal, S.M. Olhero and Budhendra Singh would like to thank the Foundation for Science and Technology of Portugal (FCT) for the financial support under corresponding grant references SFRH/BPD/77598/2011, SFRH/BPD/87486/2012 and SFRH/BPD/76184/2011, respectively. D. Fagg acknowledges funding from FCT under grant PTDC/CTM/105424/2008, FEDER and COMPETE. The authors would also like to thank CICECO for the work at the University of Aveiro.

## References

- [1] W. Liu, X. Ren, Large piezoelectric effect in Pb-free ceramics, *Phys. Rev. Lett.* 103 (2009) 257602 (–257602).
- [2] A. Kaushal, S.M. Olhero, J.M.F. Ferreira, Lead-free  $0.5\text{Ba}(\text{Zr}_{0.2}\text{Ti}_{0.8})\text{O}_3-0.5(\text{Ba}_{0.7}\text{Ca}_{0.3})\text{TiO}_3$  powder surface treated against hydrolysis — a key for a successful aqueous processing, *J. Mater. Chem. C* 1 (2013) 4846–4853.
- [3] D. Xue, Y. Zhou, H. Bao, J. Gao, C. Zhou, X. Ren, Large piezoelectric effect in Pb-free  $\text{Ba}(\text{Ti},\text{Sn})\text{O}_3-x(\text{Ba},\text{Ca})\text{TiO}_3$  ceramics, *Appl. Phys. Lett.* 99 (2011) 122901–122903.
- [4] P. Mishra, Sonia P. Kumar, Effect of sintering temperature on dielectric, piezoelectric and ferroelectric properties of BZT–BCT 50/50 ceramics, *J. Alloys Comp.* 545 (2012) 210–215.
- [5] S. Su, R. Zuo, S. Lu, Z. Xu, X. Wang, L. Li, Poling dependence and stability of piezoelectric properties of  $\text{Ba}(\text{Zr}_{0.2}\text{Ti}_{0.8})\text{O}_3-(\text{Ba}_{0.7}\text{Ca}_{0.3})\text{TiO}_3$  ceramics with huge piezoelectric coefficients, *Curr. Appl. Phys.* 11 (2011) S120–S123.
- [6] V.S. Puli, D.K. Pradhan, W. Pérez, R.S. Katiyar, Structure, dielectric tunability, thermal stability and diffuse phase transition behavior of lead free BZT–BCT ceramic capacitors, *J. Phys. Chem. Solids* 74 (2013) 466–475.
- [7] W. Wu, L. Cheng, S. Bai, W. Dou, Q. Xu, Z. Wei, Y. Qin, Electrospinning lead-free  $0.5\text{Ba}(\text{Zr}_{0.2}\text{Ti}_{0.8})\text{O}_3-0.5(\text{Ba}_{0.7}\text{Ca}_{0.3})\text{TiO}_3$  nanowires and their application in energy harvesting, *J. Mater. Chem. A* 1 (2013) 7332–7338.
- [8] A.B. Haugen, J.S. Forrester, D. Damjanovic, B. Li, K.J. Bowman, J.L. Jones, Structure and phase transitions in  $0.5(\text{Ba}_{0.7}\text{Ca}_{0.3})\text{TiO}_3-0.5(\text{BaZr}_{0.2}\text{Ti}_{0.8}\text{O}_3)$  from  $-100^\circ\text{C}$  to  $150^\circ\text{C}$ , *J. Appl. Phys.* 113 (2013) 014103–014107.
- [9] J.R. Macdonald, Impedance spectroscopy, *Ann. Biomed. Eng.* 20 (1992) 289–305.
- [10] S. Sen, R.N.P. Choudhary, A. Tarafdar, P. Pramanik, Impedance spectroscopy study of strontium modified lead zirconate titanate ceramics, *J. Appl. Phys.* 99 (2006) 124114–124121.
- [11] K. Rundgren, O. Lyckfeldt, M. Sjöstedt, Improving powders with freeze granulation, *Ceram. Ind.* 153 (2003) 40–44.
- [12] O. Lyckfeldt, D. Käck, K. Rundgren, Pressing and sintering developments of Freeze Granulated  $\text{Si}_3\text{N}_4$  materials, *Ceram. Eng. Sci. Proc.* 24 (2003) 331–336.
- [13] O. Lyckfeldt, K. Rundgren, M. Sjöstedt, Freeze Granulation for the Processing of Silicon Nitride Ceramics, *Key Engineering Materials, Key Engineering Materials*, 2004, 264–268 [Part 1] 281–284.
- [14] Q. Wang, S.M. Olhero, J.M.F. Ferreira, W. Cui, K. Chen, Z. Xie, Hydrolysis control of AlN powders for the aqueous processing of spherical AlN granules, *J. Am. Ceram. Soc.* 96 (2013) 1383–1389.
- [15] A. Kaushal, S.M. Olhero, B.K. Singh, Reza Zamiri, V. Saravanan, J.M.F. Ferreira, Synthesis and aqueous processing of lead free piezoelectric  $0.5\text{Ba}(\text{Zr}_{0.2}\text{Ti}_{0.8})\text{O}_3-0.5(\text{Ba}_{0.7}\text{Ca}_{0.3})\text{TiO}_3$  ceramics: the benefits of freeze granulation on final properties, *J. Eur. Ceram. Soc.* (2014) (Submitted for publication).
- [16] A. Kaushal, S.M. Olhero, P. Antunes, A. Ramalho, J.M.F. Ferreira, Structural, mechanical and dielectric properties of  $\text{Ba}_{0.6}\text{Sr}_{0.4}\text{TiO}_3$  — the benefits of a colloidal processing approach, *Mater. Res. Bull.* 50 (2014) 329–336.
- [17] C.F. Yang, Improvement of the sintering and dielectric characteristics of surface barrier layer capacitors by CuO addition, *Jpn. J. Appl. Phys.* 35 (1996) 1806–1813.
- [18] A.K. Jonscher, The ‘universal’ dielectric response, *Nature* 267 (1977) 673–679.
- [19] D.C. Sinclair, A.R. West, Impedance and modulus spectroscopy of semiconducting  $\text{BaTiO}_3$  showing positive temperature coefficient of resistance, *J. Appl. Phys.* 66 (1989) 3850–3856.
- [20] D.C. Sinclair, A.R. West, Effect of atmosphere on the PTCR properties of  $\text{BaTiO}_3$  ceramics, *J. Mater. Sci.* 29 (1994) 6061–6068.
- [21] B.K. Singh, B. Kumar, Impedance analysis and high temperature conduction mechanism of flux grown  $\text{Pb}(\text{Zn}_{1/3}\text{Nb}_{2/3})_{0.91}\text{Ti}_{0.09}\text{O}_3$  single crystal, *Cryst. Res. Tech.* 45 (2010) 1003–1011.
- [22] S.P. Singh, A.K. Singh, D. Pandey, H. Sharma, O. Parkash, Crystallographic phases, phase transitions and barrier layer formation in  $(1-x)[\text{Pb}(\text{Fe}_{1/2}\text{Nb}_{1/2})\text{O}_3]-x\text{PbTiO}_3$ , *J. Mater. Res.* 18 (2003) 2677–2687.
- [23] M.A.L. Nobre, S. Lanfredi, Dielectric properties of  $\text{Bi}_3\text{Zn}_2\text{Sb}_3\text{O}_{14}$  ceramics at high temperature, *Mater. Lett.* 47 (2001) 362–366.
- [24] M.A.L. Nobre, S. Lanfredi, Thermistor ceramic with negative temperature coefficient based on  $\text{Zn}_7\text{Sb}_2\text{O}_{12}$ : An inverse spinel-type phase, *Appl. Phys. Lett.* 81 (2002) 451–453.
- [25] A.K. Jonscher, *Dielectric Relaxation in Solids*, Chelsea Dielectrics press, London, 1983.
- [26] R. Schmidt, W. Eerenstein, P.A. Midgley, Large dielectric response to the paramagnetic-ferromagnetic transition ( $\text{TC} \sim 100\text{ K}$ ) in multiferroic  $\text{BiMnO}_3$  epitaxial thin films, *Phys. Rev. B* 79 (2009) 214107–214111.
- [27] N. Narendar, G.C. Mather, P.A.N. Dias, D.P. Fagg, The importance of phase purity in  $\text{Ni}-\text{BaZr}_{0.85}\text{Y}_{0.15}\text{O}_{3-\delta}$  cermet anodes — novel nitrate-free combustion route and electrochemical study, *RSC Adv.* 3 (2013) 859–869.
- [28] F.D. Morrison, D.C. Sinclair, A.R. West, Characterization of lanthanum-doped barium titanate ceramics using impedance spectroscopy, *J. Am. Ceram. Soc.* 84 (2001) 531–538.
- [29] P. Balaya, J. Jamnik, J. Fleig, J. Maier, Mesoscopic electrical conduction in nanocrystalline  $\text{SrTiO}_3$ , *Appl. Phys. Lett.* 88 (2006) 062109–062111.
- [30] J. Zheng, J.S. Reed, Particle and granule parameters affecting compaction efficiency in dry pressing, *J. Am. Ceram. Soc.* 71 (11) (1988) C456–C458.
- [31] I.M. Hodge, M.D. Ingram, A.R. West, Impedance and modulus spectroscopy of polycrystalline solid electrolytes, *J. Electroanal. Chem.* 74 (1976) 125–143.
- [32] M.A.L. Nobre, S. Lanfredi, Phase transition in sodium lithium niobate polycrystal: an overview based on impedance spectroscopy, *J. Phys. Chem. Solids* 62 (2001) 1999–2006.
- [33] J.T.S. Irvine, D.C. Sinclair, A.R. West, Electroceramics: characterization by impedance spectroscopy, *Adv. Mater.* 2 (1990) 132–138.